The Astrophysical Journal Letters, 881:L8 (6pp), 2019 August 10 https://doi.org/10.3847/2041-8213/ab3041

Energetic Electron Acceleration in Unconfined Reconnection Jets

G. Chen[1,2,3], H. S. Fu[4], Y. Zhang[1,2,3], Xiaocan Li[5], Y. S. Ge[1,2,3], A. M. Du[1,2,3], C. M. Liu[4], and Y. Xu[4]
[1] Key Laboratory of Earth and Planetary Physics, Institute of Geology and Geophysics, Chinese Academy of Sciences, Beijing 100029, People's Republic of China
[2] Institutions of Earth Science, Chinese Academy of Sciences, Beijing 100029, People's Republic of China
[3] University of Chinese Academy of Sciences, Beijing 100049, People's Republic of China
[4] School of Space and Environment, Beihang University, Beijing 100083, People's Republic of China; huishanf@gmail.com
[5] Los Alamos National Laboratory, Los Alamos, NM 87545, USA
Received 2019 May 15; revised 2019 July 3; accepted 2019 July 8; published 2019 August 5

Abstract

Magnetic reconnection in astronomical objects such as solar corona and the Earth's magnetotail theoretically produces a fast jet toward the object (known as a confined jet as it connects to the object through magnetic field lines) and a fast jet departing the object (known as an unconfined jet as it propagates freely in space). So far, energetic electron acceleration has been observed in the confined jet but never in the unconfined jet, arousing a controversy about whether or not reconnection jets can intrinsically accelerate electrons. By analyzing spacecraft measurements in the magnetotail, here we report three events showing strong electron energization in unconfined reconnection jets. Such energization, occurring in the growing phase of the jet, is quasi-adiabatic; it leads to 30 times of flux enhancements and it is probably caused by the compression of the magnetic field (betatron effect) as well as the shrinking of magnetic field lines (Fermi effect). We quantitatively reproduce this energization process using a 2.5D particle-in-cell simulation. This finding implies that electron acceleration can happen in the solar wind and magnetosheath, where reconnection jets are usually unconfined.

Key words: acceleration of particles – magnetic reconnection

1. Introduction

Magnetic reconnection is a fundamental plasma process explosively converting magnetic energy into particle energy in the forms of fast jets and energetic electrons (Vasyliunas 1975; Fu et al. 2017). Such a process can happen in the solar corona (Shibata et al. 1995) and solar wind (Phan et al. 2006; Zhang et al. 2008), in the Earth's magnetotail (Fu et al. 2013a; Torbert et al. 2018; Lu et al. 2019b) and magnetosheath (Retinò et al. 2007; Chen et al. 2018; Guo et al. 2018), and at the Earth's magnetopause (Burch et al. 2016; Fu et al. 2019a). Magnetic reconnection in the solar corona and the Earth's magnetotail theoretically generates a fast plasma jet toward the Sun/Earth, which hits the solar photosphere or the Earth's atmosphere to produce the solar flare (Shibata et al. 1995) or aurora (Angelopoulos et al. 2008), and a fast plasma jet departing the Sun/Earth, which acts as an outward solar eruption (Shibata et al. 1995) or a tailward bursty bulk flow (Angelopoulos et al. 1994; Cao et al. 2006, 2013; Du et al. 2011; Zhao et al. 2016; Chen et al. 2019). This pair of plasma jets has quite different properties: the jet toward the Sun/Earth is connected to the object through magnetic field lines, so it is a confined jet (Figure 1(a)); the jet departing the Sun/Earth propagates freely in space, so it is an unconfined jet (Figure 1(a)). Unlike the reconnection in the solar corona and the Earth's magnetotail, the reconnection at the Earth's magnetopause and in the solar wind always produces a pair of unconfined jets (Figure 1(b)).

For many years, reconnection jets have been suggested to account for electron acceleration (Hoshino et al. 2001; Zenitani & Hoshino 2001; Huang et al. 2015; Lu et al. 2016a, 2018, 2019a). However, such acceleration was only observed in the confined jets, such as the earthward outflow (Hoshino et al. 2001; Imada et al. 2007; Wang et al. 2010; Ashour-Abdalla et al. 2011; Fu et al. 2011, 2013b, 2019b; Ge et al. 2011; Vaivads et al. 2011; Huang et al. 2012; Lu et al. 2015, 2016b; Liu et al. 2017a, 2017b, 2017c; Xu et al. 2018a, 2018b; Liu & Fu 2019) and the solar flare (Somov & Kosugi 1997; Aschwanden 2002; Lin et al. 2003). In these regions, energetic electrons can be trapped in a magnetic flux tube whose footprints (Figure 1(a)) are at the surface of the Sun/Earth, and subsequently the electrons gain energy during the shrinking of magnetic field lines (Fermi effect; Fu et al. 2011) and the compression of the magnetic field (betatron effect; Fu et al. 2011). So far, there has been no evidence of electron acceleration in the unconfined reconnection jets in the solar wind (Gosling et al. 2005) and in the magnetotail. Thus, it is still a puzzle whether reconnection jets can intrinsically accelerate energetic electrons. Notice that some previous studies (e.g., Wu et al. 2015; Zhou et al. 2016) reported energetic electrons in the tailward flow in the Earth's magnetotail, but the fluxes of those electrons are extremely low (1/1000 of the fluxes in the earthward flow), which cannot be indisputably regarded as the evidence of energetic electrons.

Here we report, for the first time, strong electron acceleration in unconfined reconnection jets, by analyzing spacecraft measurements in the Earth's magnetotail. The unconfined jets are three tailward flows with speed higher than 600 km s^{-1}.

2. Observations

The first event was detected by *Cluster* (Escoubet et al. 2001) on 2001 September 15 at 03:30–03:50 UT, when the spacecraft was located at (−18.8, 3.56, −1.50) R_E in the Earth's magnetotail, with separations of ∼2000 km. Specifically, C3 was closer to the plasma sheet center than C1, because it measured very weak magnetic fields ($B_X < 2$ nT; see Figure 2(b)). Before 03:40 UT (left vertical dashed line in Figures 2(a)–(l)), both spacecraft detected a very quiet plasma sheet that was characterized by steady magnetic fields (Figures 2(a) and (b)) and super-small flow velocities (Figures 2(c) and (d)), while after 03:40 UT they detected a bursty bulk flow (Figures 2(c) and (d)). This flow, lasting for 7 minutes (03:40–03:47 UT), was produced by magnetotail reconnection. It had a velocity in the $-X_{GSM}$

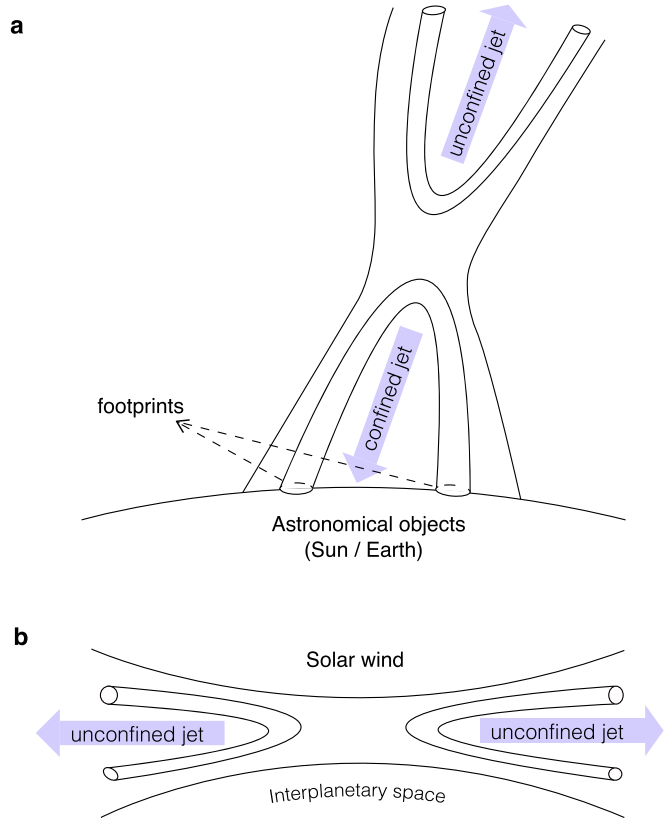

Figure 1. Sketch of the two types of reconnection jets. (a) Magnetic reconnection in an astronomical object such as the Sun or the Earth. Such reconnection can produce a fast jet toward the object—known as a confined jet as it connects to the object through magnetic field lines—and a fast jet departing the object—known as an unconfined jet as it propagates freely in space. (b) Magnetic reconnection in the solar wind or magnetosheath, which produces a pair of unconfined jets.

direction (Figures 2(c) and (d)), meaning that it was a tailward reconnection jet departing the Earth. Such a tailward jet, with no connection to the Earth, can propagate freely in space, and thus can be identified as an unconfined reconnection jet (see Figure 1(a)).

This unconfined jet includes two phases: the "growing phase" from 03:40 to 03:45 UT (see the gray shades in Figures 2(c) and (d))—characterized by flow-velocity increase ($|V_X|$ from 0 to 600 km s^{-1}) and the "decaying phase" from 03:45 to 03:47 UT—characterized by flow-velocity decrease ($|V_X|$ from 600 km s^{-1} to 0; see Figures 2(c) and (d); Fu et al. 2012a; Zhao et al. 2019). Considering the frozen-in condition, which is satisfied when reconnection jets leave the ion diffusion region (Fu et al. 2012b, 2019c; Peng et al. 2017; Liu et al. 2018a, 2018b), these two phases have different behaviors: in the growing phase, the flow velocity increases, which leads to compression of magnetic flux tubes and consequently the strengthening of magnetic fields (Fu et al. 2011); in the decaying phase, the flow velocity decreases, which leads to expansion of flux tubes and consequently the weakening of magnetic fields (Fu et al. 2011). Such different behaviors may result in different electron-acceleration processes (Fu et al. 2011).

In this event, electron acceleration was indeed observed. Such acceleration, elevating electron energy to 127 keV (Figures 2(e) and (f)), exhibited a good correlation with the flow velocity (Figures 2(c) and (d)): when flow velocity was small (before 03:40 UT and after 03:47 UT) or decreasing (03:45−03:47 UT), no clear electron acceleration was observed; when flow velocity was increasing (03:40−03:45 UT), strong electron acceleration was observed. In contrast, it did not exhibit correlation with the magnetic field (Figures 2(a) and (b)), meaning that the electron acceleration in this event was attributed to the flow velocity rather than magnetic field.

The energetic electrons appeared primarily in the growing phase of the jet (Figures 2(e) and (f)) rather than at the flow peak (03:45 UT), indicating that these energetic electrons were accelerated locally but not transported from the reconnection site. In other words, if the energetic electrons were accelerated near the reconnection site and then transported along with the reconnection outflow, they should appear near the flow peak (see the discussion by Liu et al. 2019). Since the acceleration is a local process, we can certainly treat the electrons measured locally in the quiet plasma sheet as the source, and we can treat the electrons measured in the growing phase of the jet as the energized population. Specifically, in this event, we treat the C3 measurements during 03:37−03:40 UT (see the long horizontal bar between Figures 2(d) and (f)) as the source, because during that period C3 was almost in the center of a quiet plasma sheet ($B_X < 2$ nT), and we treat the C3 measurements during 03:42:00−03:42:30 UT (see the short horizontal bar between Figures 2(d) and (f)) as the energized population, because during that period electron fluxes were the highest (Figure 2(f)).

Figures 2(g) and (h) show the pitch angle distribution (PAD) of both the source and energized populations, while Figures 2(m)–(o) present the phase space density (PSD) of these two populations in the omni, field-aligned, and perpendicular directions, respectively. Interestingly, the PAD of the energized population was isotropic from 0° to 180° with no enhancement of electron fluxes at any pitch angles (Figures 2(g) and (h)). Such isotropic PAD is a consequence of wave–particle interactions in most of the events (e.g., Fu et al. 2014; Cao et al. 2017; Wang et al. 2019; Wei et al. 2007) but not in this event. In the present event, the electron acceleration should be adiabatic because (1) both the source and energized populations exhibited power-law distributions PSD $\propto \varepsilon^{-\gamma}$ with similar index $\gamma \approx 3.7$ (see Figures 2(m)–(o)); (2) no clear wave emissions were observed during the electron acceleration (see Figures 2(i) and (j)). Such an adiabatic process is traditionally referred to as the betatron mechanism, which elevates electron speed uniformly in the perpendicular direction and leads to flux enhancement in the perpendicular direction, and the Fermi mechanism, which elevates electron speed uniformly in the field-aligned direction and leads to flux enhancement in the parallel and antiparallel directions. Since the flux enhancement covered all the pitch angles (from 0° to 180°) in this event (Figures 2(g) and (h)), both the betatron and Fermi mechanisms should be involved. These two mechanisms worked together to enhance the electron fluxes by 30 times (see Figures 2(m)–(o)).

We can quantify the acceleration efficiency in the framework of Liouville's theorem, which requires the PSD to be a constant during acceleration (Egedal et al. 2010; Liu et al. 2017b, 2019). Specifically, we move the distribution function of the source population (black solid lines in Figures 2(m)–(o)) along a constant PSD rightward to achieve the energization. We find that, in all the omni, field-aligned, and perpendicular directions, the adiabatic acceleration, with energy uniformly elevated by 1.5 times ($E_2/E_1 = 2.5$ at all energy channels), can make the modeling result (red dashed lines in Figures 2(m)–(o)) agree

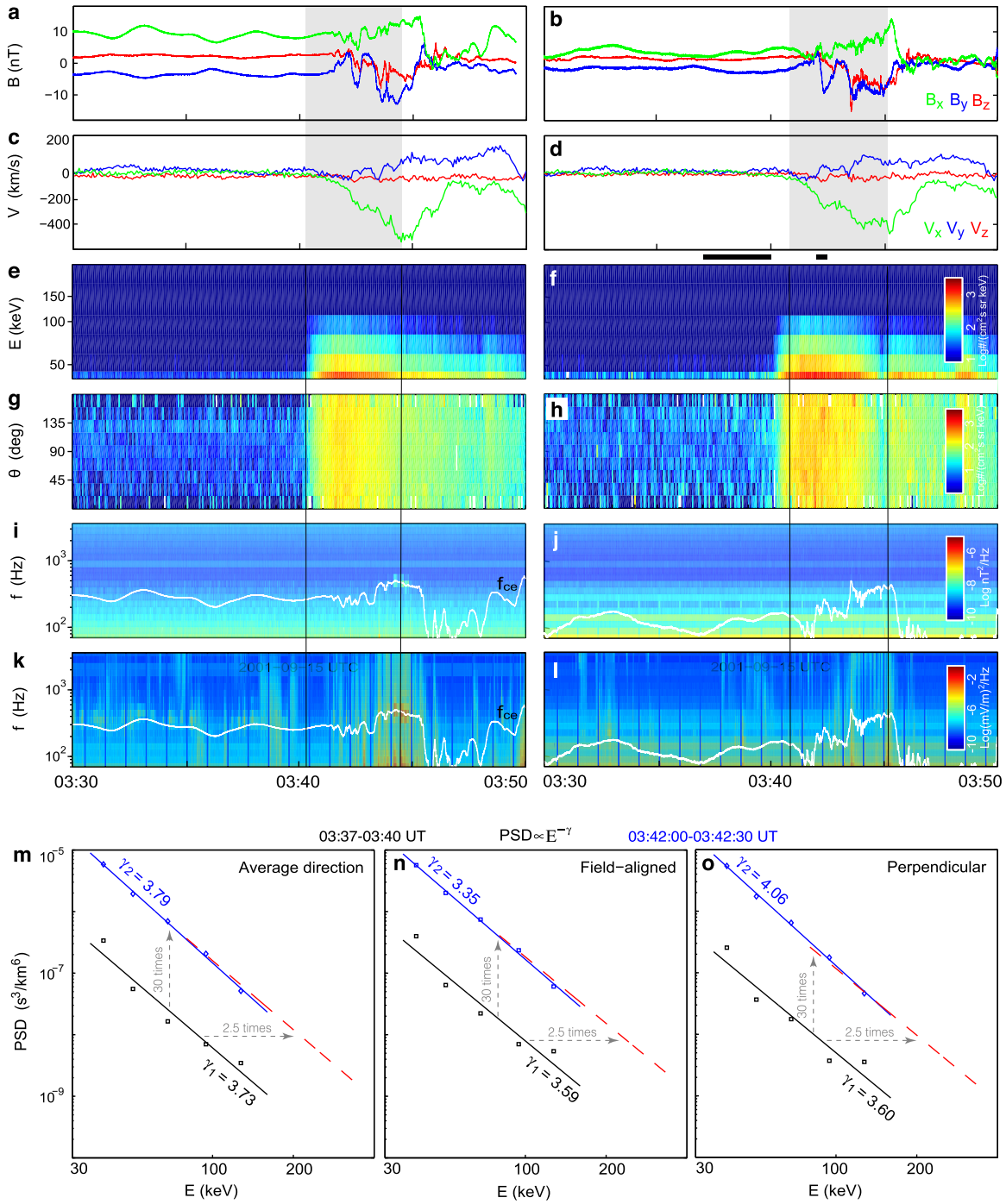

Figure 2. *Cluster* measurements of electron acceleration in unconfined reconnection jets on 2001 September 15. ((a)–(b)) The magnetic field. ((c)–(d)) The ion bulk velocity. ((e)–(f)) Differential particle flux (DPF) of the 40–250 keV electrons. ((g)–(h)) Pitch angle distribution of the 40–250 keV electrons. ((i)–(l)) Power spectra density of the magnetic field and electric field, with the white line denoting the electron cyclotron frequency. ((m)–(o)) Phase space density (PSD) of the 40–128 keV electrons in the average, field-aligned, and perpendicular directions. The black squares represent the source population measured by C3 during 03:37:00–03:40:00 UT, while the blue squares represent the energized population measured by C3 inside the growing phase of the jet. The black and blue solid lines are the fittings of spacecraft measurements, while the red dashed lines are the modeling results based on Liouville's theorem. Data are presented in GSM coordinates. The left column, panels (a), (c), (e), (g), (i), (k), shows the C1 measurements, while the right column, panels (b), (d), (f), (h), (j), (l), shows the C3 measurements.

well with the measurements in the growing phase of the jet (blue solid lines in Figures 2(m)–(o)). This means that the acceleration processes in this event, including both the Fermi (Figure 2(n)) and betatron (Figure 2(o)) mechanisms, can energize electrons by 1.5 times, which is very efficient, compared to most of the electron acceleration by magnetic reconnection (Fu et al. 2019b).

We can find two more events, exhibiting electron-acceleration features in the growing phase of unconfined reconnection jets, as shown in Figure 3. These two events, detected by C1 on 2001 October 11 and 2005 September 26, respectively, both happened in the midtail region ($X_{\rm GSM} \approx -16\,R_{\rm E}$). In both events, the tailward flows with ion velocity up to $V_X = -800\,{\rm km\,s^{-1}}$ or $V_X = -1200\,{\rm km\,s^{-1}}$ (unconfined reconnection jets) were observed

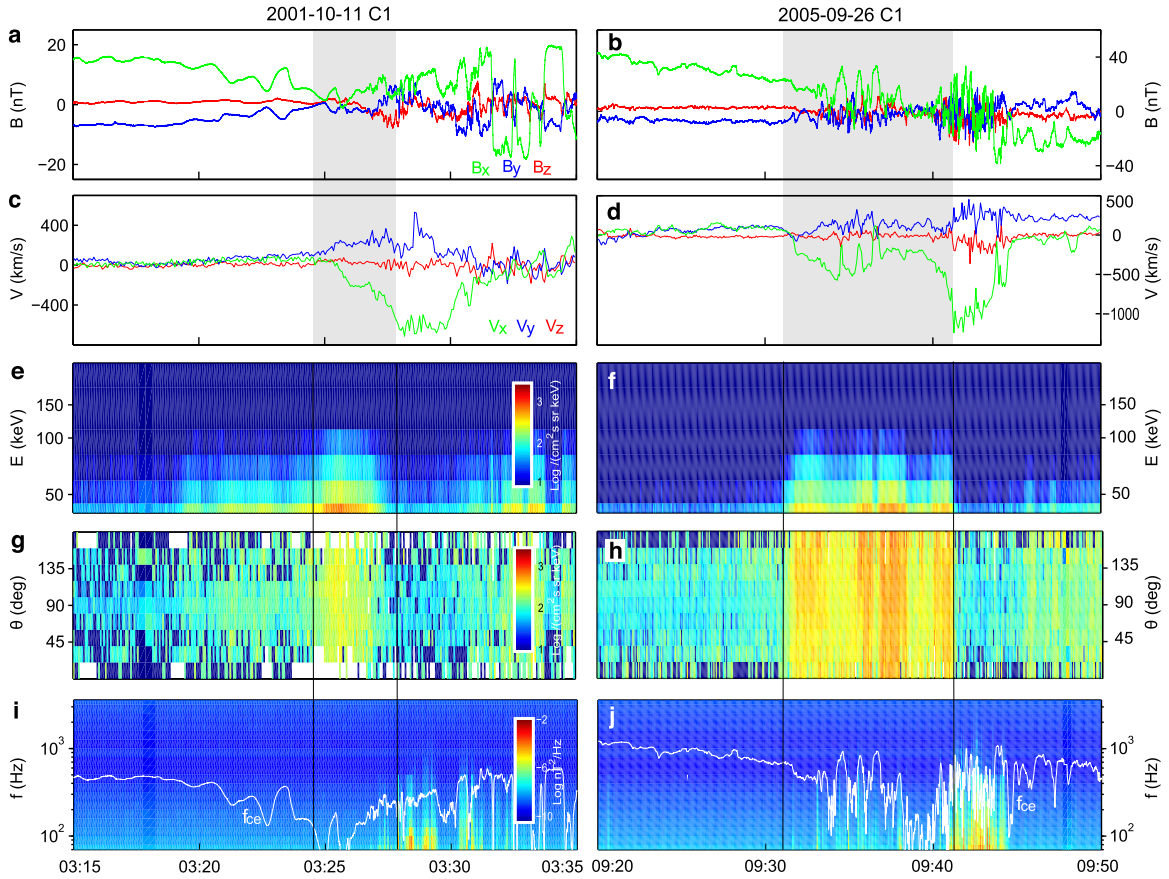

Figure 3. The other two events showing electron acceleration in unconfined reconnection jets, measured by *Cluster* 1 in the magnetotail on 2001 October 11 and 2005 September 26. ((a)–(b)) Magnetic field. ((c)–(d)) Ion bulk velocity. ((e)–(f)) DPF of the 40–250 keV electrons. ((g)–(h)) Pitch angle distribution of 40–68 keV electrons. ((i)–(j)) Power spectral density of the magnetic field, overplotted with the electron cyclotron frequency (white line).

(Figures 3(c) and (d)). Such reconnection jets, similarly, had a growing phase and a decaying phase (Figures 3(c) and (d)). The electron energization appeared only in the growing phase; it elevated electron energy up to 127 keV (Figures 3(e) and (f)). Such energization was adiabatic because no wave emissions were observed during the acceleration (Figures 3(i) and (j)). However, it resulted in an isotropic PAD of energetic electrons (see Figures 3(g) and (h)), meaning that both the Fermi and betatron mechanisms were involved. All these features, including the electron acceleration during flow increase (Figures 3(e) and (f)), the absence of waves (Figures 3(i) and (j)), and the isotropic distributions (Figures 3(g) and (h)), are similar to those in event 2001 September 15, manifesting that such a phenomenon is not unique. Instead, it should happen commonly in the Earth's magnetotail, and should probably happen in the solar corona, at the magnetopause, and in the solar wind.

It is reasonable to expect betatron acceleration of electrons in the growing phase of reconnection jets because during flow velocity increase magnetic flux tubes are compressed and consequently magnetic fields are strengthened, which results in electron energization in the perpendicular direction under the condition that the first adiabatic invariant $\mu \sim V_\perp^2/B$ is conserved (Fu et al. 2011). Fermi acceleration happening in an unconfined reconnection jet is also possible: during the propagation of a reconnection outflow, a pair of mirror points can be formed near the separatrix region (Hoshino et al. 2001), although the magnetic field lines do not connect to any object (e.g., Sun or Earth). As a result, electrons will be trapped and bounce between these two mirror points. Since the leading part of the flow moves more slowly than the trailing part, the magnetic field lines between the two mirror points actually are shortening, which leads to electron energization in the parallel and antiparallel directions under the condition that the second adiabatic invariant $J = \int_0^L v_{//} dl$ is conserved (Fu et al. 2011). These two processes (betatron and Fermi acceleration) worked together to produce the isotropic PAD of electrons in these events (Figures 2(g) and (h); Figures 3(g) and (h)).

3. Simulations

We perform a 2.5D vector particle-in-cell (VPIC) simulation (Bowers et al. 2008; Li et al. 2015, 2017) to examine whether such phenomenon—electron acceleration in unconfined reconnection jets—can happen. We use the C3 measurements during 03:37–03:40 UT (on 2001 September 15) in the plasma sheet center as the initial condition and consider an open boundary condition (Liu et al. 2014; Li et al. 2018a, 2018b). The simulation box is $60d_i \times 20d_i$ in the XZ plane. At $t = 30\omega_{ci}$, B_X is positive at $Z > 0$ but negative at $Z < 0$ (Figure 4(a)), resembling the northern and southern hemispheres of the Earth's magnetotail. B_Y exhibits a quadrupolar pattern (Figure 4(b)), which can be interpreted as the Hall magnetic field. A pair of reconnection jets, with a velocity up to $|V_X| = 0.06$, are produced in opposite directions (Figure 4(c)). Since we use an open boundary condition, these reconnection jets are unconfined, hence satisfying our requirements. To compare with the observations on 2001 September 15, when *Cluster* was in the northern hemisphere and measured positive B_X (Figures 2(a) and (b)), we consider a virtual spacecraft crossing the simulation box from $X = 30d_i$ to $X = 0$

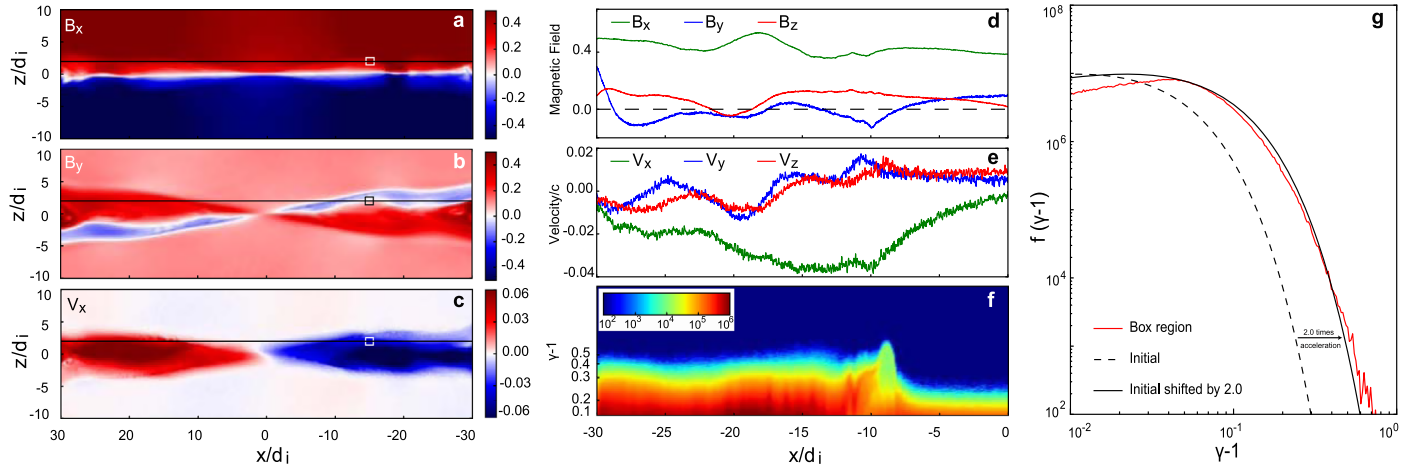

Figure 4. VPIC simulation of electron acceleration in unconfined reconnection jets. The C3 measurements during 03:37–03:40 UT on 2001 September 15 are used as the initial condition, and the open boundary condition is used. ((a)–(c)) The magnetic field B_X and B_Y, and the ion velocity V_X at $t = 30\omega_{ci}$; ((d)–(f)) the magnetic field, ion velocity, and electron energy spectrogram along the cut line in panels (a)–(c) from $X = -30d_i$ to $X = 0$. (g) The electron flux at the initial state (black dashed line) and $t = 30\omega_{ci}$ (red solid line), taken from the small box in panels (a)–(c). The black solid line is a modeling result based on Liouville's theorem.

along the cut line at $Z = 2d_i$ (see the black line in Figures 4(a)–(c)). The simulation results along this cut line, including magnetic fields, ion flow velocities, and the electron energy spectrogram, are shown in Figures 4(d)–(f) respectively. We find that both the magnetic fields (Figure 4(d)) and ion flow velocities (Figure 4(e)) are similar to those measured by C3 (Figures 2(b) and (d)). A tailward jet ($V_X < 0$), including a growing phase (from $V_X \approx 0$ to $V_X \approx -0.04$) and a decaying phase (from $V_X \approx -0.04$ to $V_X \approx 0$), is captured (Figure 4(e)). The energetic electrons ($\gamma - 1 > 0.25$) only appear in the growing phase of the jet (see Figure 4(f)), well consistent with the spacecraft observations (Figure 2(f)).

We focus on a specific snapshot measured by the virtual spacecraft to analyze the acceleration process, as that done in Figure 2(m). This snapshot, containing particles in a $1d_i \times 1d_i$ box, is taken from the position $(-15, 2)\ d_i$ (see the small box in Figures 4(a)–(c)). Figure 4(g) presents the electron distribution functions in this small box at $t = 30\omega_{ci}$ (after acceleration; see the red line) and at $t = 0$ (initial state; see the black dashed line). Generally, the distribution functions before and after acceleration are similar. If we shift the distribution function at the initial state (black dashed line) along a constant PSD (Liouville's theorem) rightward one time, the resultant distribution function (black solid line) can well match the distribution function at $t = 30\omega_{ci}$ (red solid line), meaning that the electrons in this simulation are energized by one time ($E_2/E_1 = 2$). Such acceleration efficiency ($E_2/E_1 = 2$) is comparable to that observed by *Cluster* on 2001 September 15 (Figure 2(m)), hence reproducing the primary acceleration features.

To validate our proposition of the acceleration mechanisms, we examine the pitch-angle distribution of energetic electrons ($\gamma - 1 > 0.25$) in Figure 5. We find that when the flow velocity is relatively stable (left side of the vertical dashed line, from $X \approx -28d_i$ to $X \approx -22d_i$; see Figure 5(a)), the electron fluxes are relatively low (Figure 5(b)) and the pitch angles are primarily in the parallel and antiparallel directions (Figure 5(c)), indicating the happening of only Fermi acceleration; when the flow velocity is increasing (right side of the vertical dashed line, from $X \approx -22d_i$ to $X \approx -10d_i$; see Figure 5(a)), the electron fluxes are relatively high (Figure 5(b)) and the pitch angles are generally isotropic (Figure 5(c)), indicating both Fermi and betatron acceleration are happening. In this way, the VPIC simulation results have

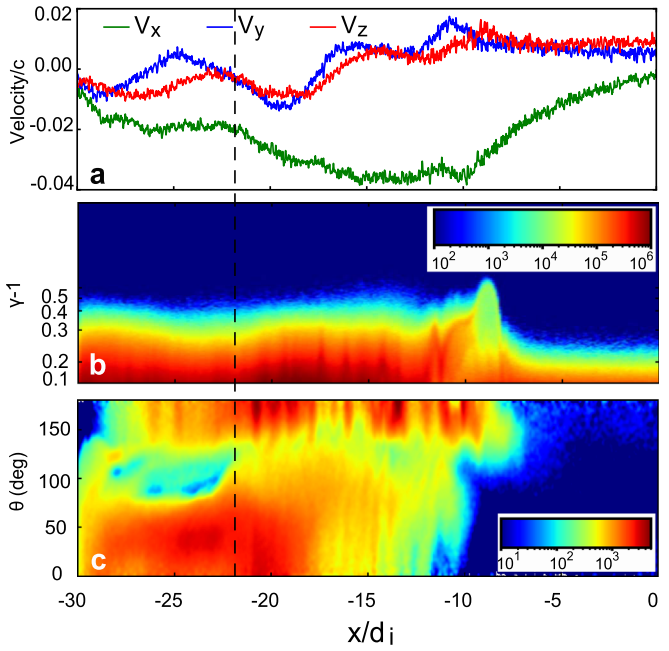

Figure 5. Ion flow velocity (a), energy spectrogram of all electrons (b), and pitch angle distribution of energetic ($\gamma - 1 > 0.25$) electrons (c) in the simulation box at $t = 30\omega_{ci}$. The vertical dashed line divides the growing phase of the flow into two parts.

quantitatively confirmed that electron acceleration can indeed happen in the growing phase of unconfined reconnection jets, and Fermi acceleration and betatron acceleration are responsible for the electron isotropic distribution.

4. Conclusions

To conclude, we report strong electron acceleration in unconfined reconnection jets. We find that such acceleration only happens in the growing phase of the jets and is caused by both the Fermi and betatron mechanisms. We quantitatively reproduce the acceleration process using a 2.5D VPIC simulation. This finding implies that electron acceleration can happen in the solar wind and magnetosheath, where reconnection jets are unconfined, resembling the tailward flow in this study.

We thank the *Cluster* Science Archive for providing the data for this study. This research was supported by NSFC grants 41874080, 41674168, 41404133, 41874188, 41574153, 40621003, and 41431071, and the Strategic Priority Research Program of the Chinese Academy of Sciences (grant No. XDA14040403).

ORCID iDs

G. Chen https://orcid.org/0000-0001-9367-0975
H. S. Fu https://orcid.org/0000-0002-4701-7219
C. M. Liu https://orcid.org/0000-0002-9705-5387
Y. Xu https://orcid.org/0000-0003-1863-7280

References

Angelopoulos, V., Kennel, C. F., Coroniti, F. V., et al. 1994, JGR, 99, 21257
Angelopoulos, V., McFadden, J. P., Larson, D., et al. 2008, Sci, 321, 931
Aschwanden, M. J. 2002, SSRv, 101, 1
Ashour-Abdalla, M., El-Alaoui, M., Goldstein, M. L., et al. 2011, NatPh, 7, 360
Bowers, K. J., Albright, B. J., Yin, L., et al. 2008, PhPl, 15, 055703
Burch, J. L., Torbert, R. B., Phan, T. D., et al. 2016, Sci, 352, 1189
Cao, D., Fu, H. S., Cao, J. B., et al. 2017, GeoRL, 44, 3954
Cao, J. B., Ma, Y. D., Parks, G., et al. 2013, JGRA, 118, 313
Cao, J. B., Ma, Y. D., Parks, G., et al. 2006, JGRA, 111, A04216
Chen, X. H., Fu, H. S., Liu, C. M., et al. 2018, ApJ, 852, 17
Chen, Z. Z., Fu, H. S., Liu, C. M., et al. 2019, GeoRL, 46, 5698
Du, A. M., Nakamura, R., Zhang, T. L., et al. 2011, JGRA, 116, A03216
Egedal, J., Lê, A., Zhu, Y., et al. 2010, GeoRL, 37, L10102
Escoubet, C. P., Fehringer, M., & Goldstein, M. 2001, AnGeo, 19, 1197
Fu, H. S., Cao, J. B., Cao, D., et al. 2019a, GeoRL, 46, 48
Fu, H. S., Cao, J. B., Cully, C. M., et al. 2014, JGRA, 119, 9089
Fu, H. S., Cao, J. B., Khotyaintsev, Y. V., et al. 2013a, GeoRL, 40, 6023
Fu, H. S., Khotyaintsev, Y. V., Andreì, M., & Vaivads, A. 2011, GeoRL, 38, L16104
Fu, H. S., Khotyaintsev, Y. V., Vaivads, A., et al. 2012a, JGRA, 117, A12221
Fu, H. S., Khotyaintsev, Y. V., Vaivads, A., et al. 2012b, GeoRL, 39, L06105
Fu, H. S., Khotyaintsev, Y. V., Vaivads, A., et al. 2013b, NatPh, 9, 426
Fu, H. S., Peng, F. Z., Liu, C. M., et al. 2019c, GeoRL, 46, 5645
Fu, H. S., Vaivads, A., Khotyaintsev, Y. V., et al. 2017, GeoRL, 44, 37
Fu, H. S., Xu, Y., Vaivads, A., & Khotyaintsev, Y. V. 2019b, ApJL, 870, L22
Ge, Y. S., Raeder, J., Angelopoulos, V., et al. 2011, JGRA, 116, A00I23
Gosling, J. T., Skoug, R. M., Haggerty, D. K., & McComas, D. J. 2005, GeoRL, 32, L14113
Guo, Z. F., Lin, Y., Wang, X. Y., et al. 2018, JGRA, 123, 9169
Hoshino, M., Mukai, T., Terasawa, T., & Shinohara, I. 2001, JGR, 106, 25979
Huang, C., Wu, M., Lu, Q., Wang, R., & Wang, S. 2015, JGRA, 120, 1759
Huang, S. Y., Vaivads, A., Khotyaintsev, Y. V., et al. 2012, GeoRL, 39, L11103
Imada, S., Nakamura, R., Daly, P. W., et al. 2007, JGRA, 112, A03202
Li, X., Guo, F., Li, H., & Birn, J. 2018a, ApJ, 855, 80
Li, X., Guo, F., Li, H., & Li, G. 2015, ApJL, 811, L24
Li, X., Guo, F., Li, H., & Li, G. 2017, ApJ, 843, 21
Li, X., Guo, F., Li, H., & Li, S. 2018b, ApJ, 866, 4
Lin, R. P., Krucker, S., Hurford, G. J., et al. 2003, ApJL, 595, L69
Liu, C. M., & Fu, H. S. 2019, ApJL, 873, L2
Liu, C. M., Fu, H. S., Cao, J. B., et al. 2017a, GeoRL, 44, 10116
Liu, C. M., Fu, H. S., Vaivads, A., et al. 2018a, GeoRL, 45, 556
Liu, C. M., Fu, H. S., Xu, Y., et al. 2017b, GeoRL, 44, 6492
Liu, C. M., Fu, H. S., Xu, Y., et al. 2017c, JGRA, 122, 594
Liu, C. M., Fu, H. S., Xu, Y., et al. 2018b, GeoRL, 45, 4628
Liu, Y.-H., Birn, J., Daughton, W., et al. 2014, JGRA, 119, 9773
Liu, Y. Y., Fu, H. S., Liu, C. M., et al. 2019, ApJL, 877, L16
Lu, S., Angelopoulos, V., Artemyev, A. V., et al. 2019a, ApJ, 878, 109
Lu, S., Angelopoulos, V., & Fu, H. 2016a, JGRA, 121, 9483
Lu, S., Artemyev, A. V., Angelopoulos, V., et al. 2016b, JGRA, 121, 4269
Lu, S., Artemyev, A. V., Angelopoulos, V., et al. 2019b, GeoRL, 46, 28
Lu, S., Lu, Q., Lin, Y., et al. 2015, JGRA, 120, 6286
Lu, S., Pritchett, P. L., Angelopoulos, V., & Artemyev, A. V. 2018, PhPl, 25, 012905
Peng, F. Z., Fu, H. S., Cao, J. B., et al. 2017, JGRA, 122, 6349
Phan, T. D., Gosling, J. T., Davis, M. S., et al. 2006, Natur, 439, 175
Retinò, A., Sundkvist, D., Vaivads, A., et al. 2007, NatPh, 3, 235
Shibata, K., Masuda, S., Shimojo, M., et al. 1995, ApJL, 451, L83
Somov, B. V., & Kosugi, T. 1997, ApJ, 485, 859
Torbert, R. B., Burch, J. L., Phan, T. D., et al. 2018, Sci, 362, 1391
Vaivads, A., Retino, A., Khotyaintsev, Y. V., & Andre, M. 2011, AnGeo, 29, 1917
Vasyliunas, V. M. 1975, RvGSP, 13, 303
Wang, R., Lu, Q., Li, X., et al. 2010, JGRA, 115, A11201
Wang, Z., Fu, H. S., Liu, C. M., et al. 2019, GeoRL, 46, 1195
Wei, X. H., Cao, J. B., Zhou, G. C., et al. 2007, JGRA, 112, A10225
Wu, M., Huang, C., Lu, Q., et al. 2015, JGRA, 120, 6320
Xu, Y., Fu, H. S., Liu, C. M., & Wang, T. Y. 2018a, ApJ, 853, 11
Xu, Y., Fu, H. S., Norgren, C., et al. 2018b, PhPl, 25, 072123
Zenitani, S., & Hoshino, M. 2001, ApJL, 562, L63
Zhang, Y., Sun, W., Feng, X. S., et al. 2008, JGRA, 113, A08106
Zhao, M. J., Fu, H. S., Liu, C. M., et al. 2019, GeoRL, 46, 2390
Zhao, Y., Wang, R. S., & Lu, Q. 2016, JGRA, 121, 10898
Zhou, M., Li, T., Deng, X., et al. 2016, JGRA, 121, 3108